DOI: 10.1002/chem.200500777

# Fine-Tuning of Properties of Bismacrocyclic Dinuclear Cyclidene Receptors by *N*-Methylation

**Sławomir Domagała,[a] Agnieszka Więckowska,[a] Jarosław Kowalski,[b] Agnieszka Rogowska,[c] Jadwiga Szydłowska,[c] Bohdan Korybut-Daszkiewicz,*[b] Renata Bilewicz,*[a] and Krzysztof Woźniak*[a]**

**Abstract:** *N*-Methylated bismacrocyclic Cu and Ni complexes were synthesised and structurally characterised in the solid state. Their properties in solution were analysed by using NMR and ESR spectroscopies and electrochemical methods. Face-to-face biscyclidenes linked through polymethylene chains form rectangular boxlike cations. These moieties can host some small guest molecules (water, π-electron donating compounds) and are stabilised by a shell of neighbouring counterions. For the bismacrocyclic dinuclear complexes containing two nickel or two copper ions, the intramolecular interactions between the metallic centres are strengthened through methylation of the macrocyclic components, as compared with the nonmethylated species. We report the electron coupling created by two unpaired electrons coming from two copper centres observed by ESR spectroscopy. Methylation weakens the electron-acceptor properties of the complexes, which leads to less effective binding of the π-electron-donating guests. It also increases the stability of the lower oxidation states. In the case of the copper complexes, both $Cu^{II}/Cu^{I}$ and $Cu^{II}/Cu^{III}$ reversible one-electron transfers are seen in the voltammograms. These changes in properties are interpreted as the consequences of steric repulsion between the methyl substituents and the macrocyclic ring.

**Keywords:** cyclidene complexes · host–guest systems · methylation · molecular recognition · supramolecular chemistry

## Introduction

Construction of molecules exhibiting controlled directional motions at the molecular level is, at present, a great scientific challenge (see references [1–4] and references therein). Such motions are realised in several model molecules, for example, bistable catenanes and rotaxane. To control molecular devices, one has to understand the factors influencing the motions and the nature of the interactions defining the mechanical bonds in model systems.

We have recently proposed[5–7] a new type of catenane consisting of bismacrocyclic transition-metal complexes linked by aliphatic chains and interlocked with a substituted crown ether. We have proved[7] that under external stimuli—electrochemical pulses—these complexes exhibit controlled intramolecular relocation of the crown ether between two positions. This relocation is possible due to π···π interactions between the aromatic fragments of the crown ether and the metal centres (Ni, Cu) embedded in the macrocyclic rings.

By changing the properties of the components of mechanically bonded molecules, one can vary the properties of the resulting complex structures. Such tuning of properties can be achieved by severe measures, for example, by replacement of the metal ions, elongation of the aliphatic linkers or change of macrocycles. On the other hand, more subtle

[a] S. Domagała, Dr. A. Więckowska, Prof. R. Bilewicz, Prof. K. Woźniak
Department of Chemistry, Warsaw University
Pasteura 1, 02-093 Warszawa (Poland)
Fax: (+48) 22-822-5996
Fax: (+48) 22-822-2892
E-mail: bilewicz@chem.uw.edu.pl
kwozniak@chem.uw.edu.pl

[b] J. Kowalski, Dr. B. Korybut-Daszkiewicz
Institute of Organic Chemistry
Polish Academy of Sciences
Kasprzaka 44/52, 01-224 Warszawa (Poland)
Fax: (+48) 22-632-6681
E-mail: bkd@icho.edu.pl

[c] A. Rogowska, Dr. J. Szydłowska
Department of Chemistry, Warsaw University
Al. Żwirki I Wigury 101, 02-089 Warszawa (Poland)

Supporting information for this article is available on the WWW under http://www.chemeurj.org/ or from the author.

  

changes to the properties can be introduced by suitable chemical modifications of particular positions of the parent systems. This strategy of fine-tuning properties is applied herein.

Busch[8] has observed in his extensive studies of "lacunar" cyclidene complexes that substitution at the bridge nitrogen atoms strongly affects the oxidation potential of coordinated metal ions. Here we describe the role of *N*-methylation in controlling the properties of bismacrocyclic substrates used for the construction of more complex molecules. The compounds investigated are shown in Scheme 1 and Figure 1.

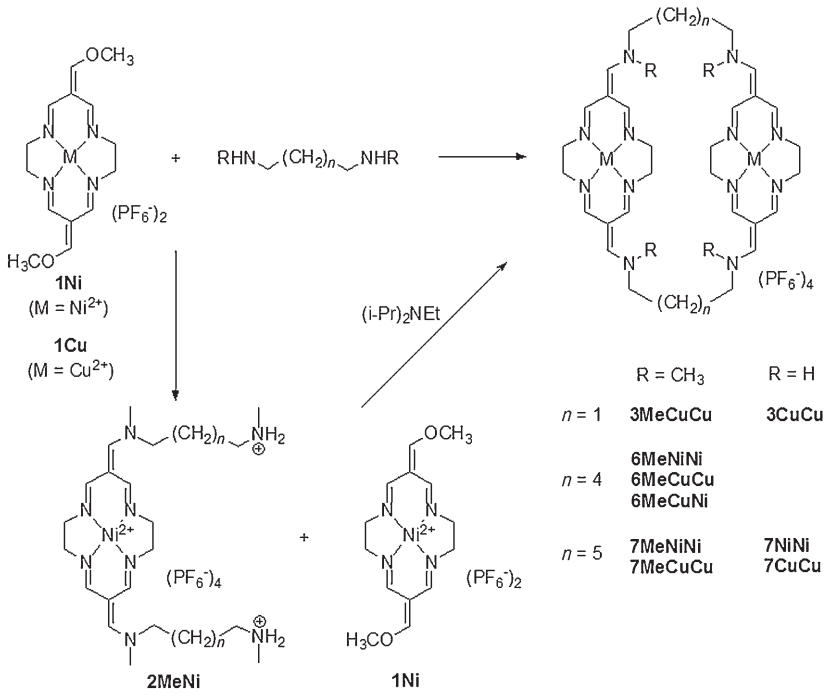


Scheme 1. Structures of cyclidene bismacrocyclic cations.

We determine the electrochemical properties of these molecules, their 3D structures and intramolecular interactions and their affinity towards selected π-donor guests (see Scheme 3).

## Experimental Section

**Synthesis**: 1,4-Bis(2-hydroxyethoxy)benzene (**1**), tetrathiafulvalene (**3**), solvents and reagents used in these studies were reagent grade or better. Acetonitrile was dried over $P_2O_5$ and distilled under argon. Hexafluorophosphate salts of **1Cu** and **1Ni** were synthesised according to the previously published procedures.[5]

***N,N*-Dimethyl-1,7-heptanediamine** was prepared by methylation of 1,7-heptanediamine according to the procedure described in the literature for another α,ω-diamine[9] (85%) and was identified by $^1$H NMR spectroscopy: $^1$H NMR ($[D_3]CH_3CN$, 200 MHz): $\delta = 1.38$ (br, 6H; γ- and δ-$CH_2$), 1.51 (s, 2H; NH), 1.54 (br m, 6H; β-$CH_2$), 2.49 (s, 6H; $CH_3$), 2.62 ppm (t, $J = 6.8$ Hz, 4H; N–$CH_2$).

**1,5-Bis(2-bromoethoxy)naphthalene (2)** was prepared according to the procedure described in literature,[10] with the modification of using acetonitrile instead of acetone as the solvent (32%). The product was identified by $^1$H NMR spectroscopy: $^1$H NMR ($[D_3]CH_3CN$, 400 MHz): $\delta = 3.85$ (t, $J = 5.5$ Hz, 4H; $CH_2Br$), 4.48 (t, $J = 5.5$ Hz, 4H; $CH_2C$), 6.95 (d, $J = 7.7$ Hz, 2H; arom.), 7.41 (t, $J = 8.0$ Hz, 2H; arom.), 7.87 ppm (d, $J = 8.0$ Hz, 2H; arom.).

**3MeCuCu**: Compound **1Cu** (0.800 g, 1.27 mmol) and *N,N*-dimethyl-1,3-propanediamine (0.159 mL, 1.27 mmol) were separately dissolved in dry acetonitrile (20 mL) and added dropwise to acetonitrile (50 mL) with a peristaltic pump at a rate of 15 $cm^3 h^{-1}$. After that, the mixture was left for 4 h at room temperature and then evaporated. The red residue was dissolved in a 1:1 mixture of acetonitrile and water and applied to a silica gel column (Merck 60 silanised, 30 × 3 cm). The column was eluted with $CH_3CN/H_2O$ (1:1) with $NH_4Cl$ (2 g per 100 mL) added. The product (the chloride salt) was collected as the first red band and excesses of NaCl and $NH_4PF_6$ were added. The organic phase was diluted with water and ethanol and slowly evaporated to give red crystals of **3MeCuCu** (0.195 g, 23%). Elemental analysis (%) calcd for $C_{34}H_{52}N_{12}Cu_2P_4F_{24}$ (1335.82): C 30.6, H 3.9, N 12.6; found: C 30.7, H 4.1, N 12.4; IR (nujol): $\tilde{\nu} = 1602$ (vs), 836 (vs), 557 $cm^{-1}$ (s); MS (ESI, $CH_3CN$): *m/z*: 188.6 ($[C_{34}H_{52}N_{12}Cu_2]^{4+}$), 299.8 ($[C_{34}H_{52}N_{12}Cu_2]^{4+} + PF_6^-$), 523.1 ($[C_{34}H_{52}N_{12}Cu_2]^{4+} + 2PF_6^-$), 1191.2 ($[C_{34}H_{52}N_{12}Cu_2]^{4+} + 3PF_6^-$).

**6MeCuCu**: Compound **1Cu** (0.630 g, 1 mmol) and *N,N*-dimethyl-1,6-hexanediamine (0.179 mL, 1 mmol) were used to perform the reaction according to the procedure as shown above. After the addition was complete, the solution was partly evaporated and a few drops of 37% HCl were instilled. The yellow solid was filtered off, washed with acetonitrile and dissolved in water (10–20 mL). The solution was absorbed on an SP Sephadex C-25 column (2 × 30 cm). The column was then washed with water and eluted with 0.5 M NaCl. The second red band was collected and the product was precipitated by addition of ammonium hexafluorophosphate. The solid was recrystallised from acetonitrile and water. The crystalline product was filtered off and dried in vacuo to give **6MeCuCu** (0.15 g, 21%). Elemental analysis (%) calcd for $C_{40}H_{64}N_{12}Cu_2P_4F_{24}\cdot H_2O$ (1437.99): C 33.4, H 4.6, N 11.7; found: C 33.2, H 4.8, N 11.6; IR (nujol): $\tilde{\nu} = 1604$ (vs), 843 (vs), 558 $cm^{-1}$ (s); MS (ESI, $CH_3CN$): *m/z*: 209.6 ($[C_{40}H_{64}N_{12}Cu_2]^{4+}$), 328.5 ($[C_{40}H_{64}N_{12}Cu_2]^{4+} + PF_6^-$), 564.2 ($[C_{40}H_{64}N_{12}Cu_2]^{4+} + 2PF_6^-$).

**6MeNiNi**: Compound **1Ni** (0.625 g, 1 mmol) and *N,N*-dimethyl-1,6-hexanediamine (0.179 mL, 1 mmol) were separately dissolved in acetonitrile and the reaction was carried out in the same way as that described above. The aqueous solution was applied to a silica gel column (Merck 60 silanised) and eluted with $CH_3CN/H_2O$ (1:7→1:1) with $NH_4Cl$ (2 g per 100 mL) added. The first major band was collected and the product was precipitated by adding ammonium hexafluorophosphate. The solid was dissolved in acetonitrile/water and crystallised by slow evaporation of the acetonitrile to give **6MeNiNi** (0.187 g, 27%). Elemental analysis (%) calcd for $C_{40}H_{64}N_{12}Ni_2P_4F_{24}$ (1410.27): C 34.1, H 4.6, N 11.9; found: C 33.9, H 4.4, N 11.7; IR (nujol): $\tilde{\nu} = 1604$ (vs), 838 (vs), 558 $cm^{-1}$ (s); MS (ESI, $CH_3CN$): *m/z*: 207.1 ($[C_{40}H_{64}N_{12}Ni_2]^{4+}$), 325.2 ($[C_{40}H_{64}N_{12}Ni_2]^{4+} + PF_6^-$); $^1$H NMR ($CD_3CN$ (mixture of conformers in solution), 500 MHz): $\delta = 1.30$–$1.50$ (m, 8H; γ-$CH_2$), 1.78 (m, 8H; β-$CH_2$), 3.34

  

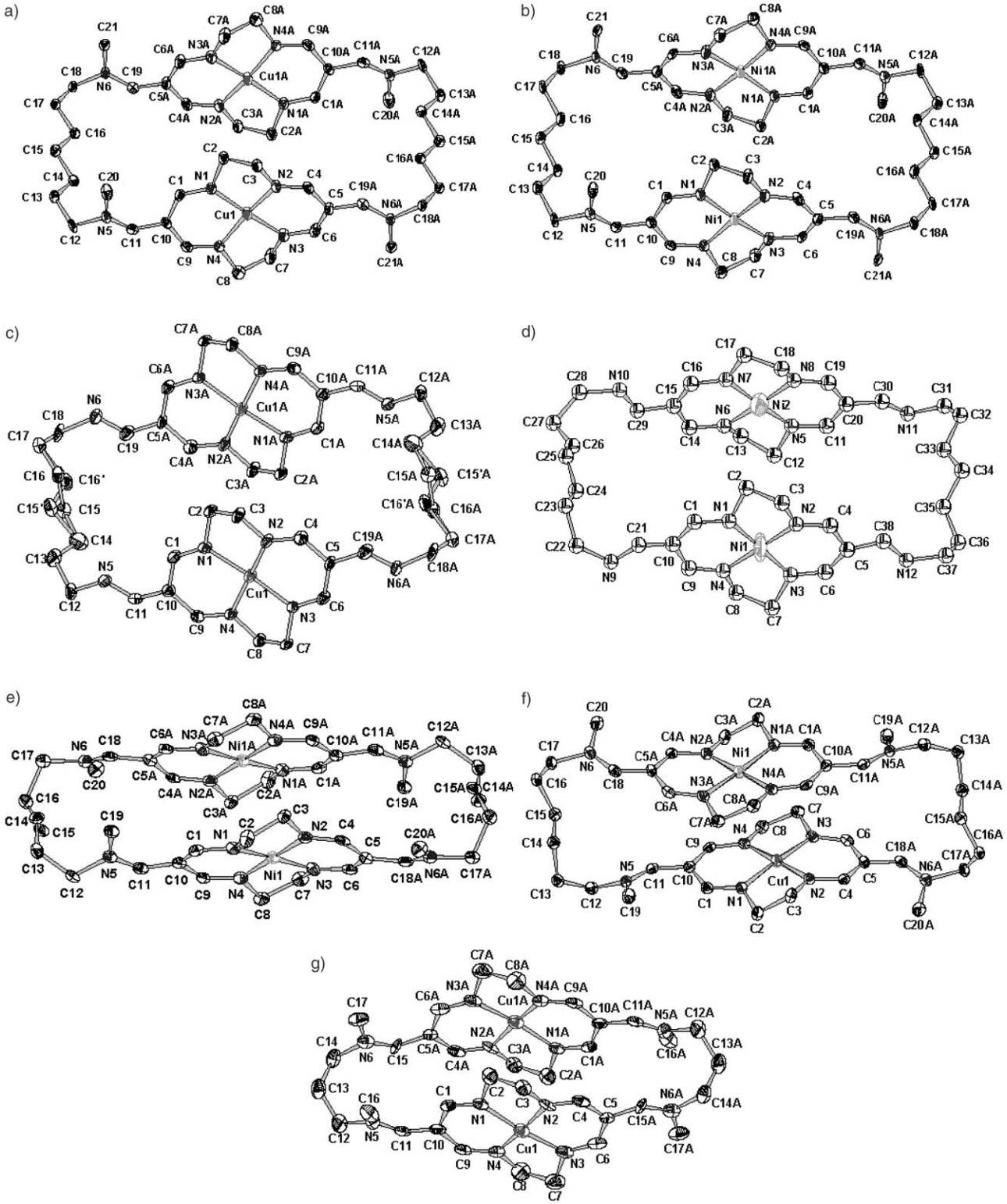


Figure 1. Structures of the compounds studied: a) **7MeCuCu**·$(PF_6^-)_4$, b) **7MeNiNi**·$(PF_6^-)_4$, c) **7CuCu**·$(PF_6^-)_4$, d) **7NiNi**·$(NO_3^-)_4$, e) **6MeNiNi**·$(PF_6^-)_4$, f) **6MeCuNi**·$(PF_6^-)_4$, g) **3MeCuCu**·$(NO_3^-)_4$.

(brs), 3.36 (brs), 3.38 (brs), 3.42 (brs, 12H; $CH_3$), 3.58–3.69 (brm, 24H; α-$CH_2$ and ring $CH_2$–$CH_2$), 7.40–8.20 ppm (several brs, 12H, CH); $^{13}$C NMR ($CD_3CN$, 125 MHz): $\delta = 24.9$, 25.7, 25.7, 26.2, 26.7, 27.0 (γ-$CH_2$), 26.1, 26.3, 27.6, 27.9, 28.1, 28.7 (β-$CH_2$), 41.0, 41.2, 41.4, 41.6 ($CH_3$ *syn*), 49.2 and 49.6 (low intensity; $CH_3$ *anti*), 54.5 (low intensity) and 54.6 (α-$CH_2$ *syn*), 62.6, 63.6, 63.7, 64.0 (α-$CH_2$ *anti*), 60.3 (br; ring $CH_2$–$CH_2$),

  

103.9, 104.4, 104.8, 104.8, 105.0 (ring C), ~156.0 and ~162 (both br; HC–N), 163.0, 163.1, 163.2, 163.4 ppm (CH–N).

**2MeNi**: *N*,*N*-Dimethyl-1,6-hexanediamine (1.34 mL, 5 mmol) dissolved in acetonitrile (25 mL) was added dropwise (at approximately 20 $cm^3 h^{-1}$) to a stirred solution of **1Ni** (0.937 g, 1.5 mmol) in acetonitrile (50 mL). After 3 h an excess of 37% hydrochloric acid (1.5 mL) was added. The yellow precipitate was filtered off, washed with acetonitrile and dissolved in water, then applied to an SP Sephadex C-25 column (2×30 cm). The column was washed with water and eluted with 0.5 M $Na_2SO_4$. The first yellow band was collected. The product precipitated upon addition of ammonium hexafluorophosphate (5 g) and was filtered off. The product was recrystallised from acetonitrile and water upon slow evaporation of solvent. The solid was dried under reduced pressure to give **2MeNi** (0.448 g, 26%). Elemental analysis: calcd (%) for $C_{28}H_{54}N_8NiP_4F_{24}$ (1141.34): C 29.5, H 4.8, N 9.8; found: C 29.5, H 4.7, N 9.8; IR (nujol): $\tilde{\nu}$=3274 (m), 1603 (vs), 844 (vs), 557 $cm^{-1}$ (s); $^1$H NMR ($CD_3CN$, 200 MHz): $\delta$=1.28–1.38 (m, 8H; γ-$CH_2$), 1.56–1.74 (m, 8H; β-$CH_2$), 2.63 (s, 6H; $CH_3$–$N^+$), 2.94 (m, 4H; $CH_2$–$N^+$), 3.33 (s, 6H; $CH_3$–N), 3.56 (br m, 12H; α-$CH_2$ and ring $CH_2$–$CH_2$), 7.58 (s, 2H; C–CH–N), 7.82 ppm (br s, 4H; N–C–H); $^{13}$C NMR ($CD_3CN$, 50 MHz): $\delta$=25.5, 25.5, 25.8, 27.8, 33.5, 63.1 ($CH_2$ of aliphatic chain), 40.9 (N–$CH_3$), 49.8 ($H_2N$–$CH_3$), 59.5 (br; ring $CH_2$–$CH_2$), 104.2 (ring C), 162.4 ppm (CH–N), HC–N not observed due to dynamic exchange.

**6MeCuNi**: Compound **1Cu** (0.214 g, 0.34 mmol), **2MeNi** (0.390 g, 0.34 mmol) and *N*-ethyldiisopropylamine (0.12 mL, 0.68 mmol) were added to stirred dry acetonitrile (50 mL). After 1 hour tetrabuthylammonium chloride (approximately 0.7 g) was added. The precipitated solid was filtered off, washed with acetonitrile (2×5 mL) and then dissolved in water (10 mL) and absorbed on a silica gel column (Merck 60 silanised). The first orange band after elution with $CH_3CN/H_2O$ (1:9→1:2) with $NH_4Cl$ (2 g per 100 mL) added was collected. The solution was treated with excesses of NaCl and $NH_4PF_6$. The organic phase was separated and diluted with water and ethanol. It then crystallised upon slow evaporation of the solvents to give **6MeCuNi** (0.045 g, 9%). Elemental analysis (%) calcd for $C_{40}H_{64}N_{12}CuNiP_4F_{24}\cdot CH_3CN$ (1456.18): C 34.6, H 4.6, N 12.5; found: C 34.9, H 4.8, N 12.6; IR (nujol): $\tilde{\nu}$=1603 (vs), 839 (vs), 559 $cm^{-1}$ (s); MS (ESI, $CH_3CN$): *m*/*z*: 208.4 ($[C_{40}H_{64}N_{12}CuNi]^{4+}$), 326.1 ($[C_{40}H_{64}N_{12}CuNi]^{4+}+PF_6^-$), 561.7 ($[C_{40}H_{64}N_{12}CuNi]^{4+}+2PF_6^-$).

**7MeCuCu**: Compound **1Cu** (0.630 g, 1 mmol) and *N*,*N*-dimethyl-1,7-heptanediamine (0.158 g, 1 mmol), both dissolved in dry acetonitrile (20 mL), were added dropwise at the rate of 15 $cm^3 h^{-1}$ (peristaltic pump) to stirred acetonitrile (50 mL). After the addition was finished, the mixture was left overnight at room temperature. The solvent was almost completely evaporated and the residue was diluted with acetonitrile/water (approximately 20 mL; 1:1). The solution was absorbed on a silica gel chromatography column (Merck 60 silanised; 3×25 cm) and eluted with acetonitrile/water (2:3→1:1) with a small amount of ammonium hexafluorophosphate (6 g per 200 mL) added. The fraction containing the first major band was treated with an excess of sodium chloride. The isolated organic phase was diluted with water and ethanol. The product crystallised upon slow evaporation of the solvents. The crystalline solid was filtered off and dried in vacuo to give **7MeCuCu** (0.268 g, 37%). Elemental analysis (%) calcd for $C_{42}H_{68}N_{12}Cu_2P_4F_{24}\cdot CH_3CN$ (1489.08): C 35.5, H 4.8, N 12.2; found: C 35.8, H 4.8, N 12.2; IR (nujol): $\tilde{\nu}$=1606 (vs), 840 (vs), 558 $cm^{-1}$ (s); MS (ESI, $CH_3CN$): *m*/*z*: 217.1 ($[C_{42}H_{68}N_{12}Cu_2]^{4+}$), 337.8 ($[C_{42}H_{68}N_{12}Cu_2]^{4+}+PF_6^-$), 579.2 ($[C_{42}H_{68}N_{12}Cu_2]^{4+}+2PF_6^-$).

**7MeNiNi**: The compound was synthesised from the nickel complex **1Ni** by following the same procedure as that above and was purified by column chromatography on silica gel (Merck 60 silanised) with acetonitrile/water (1:1) containing $NH_4PF_6$ (6 g per 200 mL) as the eluent to give **7MeNiNi** (0.227 g, 32%). Elemental analysis (%) calcd for $C_{42}H_{68}N_{12}Ni_2P_4F_{24}\cdot CH_3CN$ (1479.38): C 35.7, H 4.8, N 12.3; found: C 36.0, H 5.0, N 12.3; IR (nujol): $\tilde{\nu}$=1504 (vs), 837 (vs), 558 $cm^{-1}$ (s); MS (ESI, $CH_3CN$): *m*/*z*: 214.1 ($[C_{42}H_{68}N_{12}Ni_2]^{4+}$), 333.8 ($[C_{42}H_{68}N_{12}Ni_2]^{4+}+PF_6^-$), 574.2 ($[C_{42}H_{68}N_{12}Ni_2]^{4+}+2PF_6^-$); $^1$H NMR ($CD_3CN$, 400 MHz): $\delta$=1.10–1.40 (m, 12H; γ- and δ-$CH_2$), 1.68 (m, 8H; β-$CH_2$), 3.31 (s, 12H; $CH_3$), 3.56 (br s, 8H; α-$CH_2$), 3.61 (m, 16H; ring $CH_2$–$CH_2$), 7.55 (s, 4H; CH–N), 7.57, 8.08 ppm (br s, 2×4H; N–C–H); $^{13}$C NMR ($CD_3CN$, 50 MHz): $\delta$=26.7, 28.0 (β- and γ-$CH_2$), 30.2 (δ-$CH_2$), 40.9 ($CH_3$), 60.2 (br; ring $CH_2$–$CH_2$), 64.2 (α-$CH_2$), 104.5 (ring C), 156.6 (br) and 162.9 (br; HC-N), 162.9 ppm (CH–N).

**X-ray diffraction**: Single crystals of all $(PF_6^-)_4$ salts were obtained by slow evaporation of acetonitrile/water solutions of the studied compounds. Tetranitrates of **7NiNi**[5] and **3MeCuCu** were precipitated from the $(PF_6^-)_4$ salt solution in acetonitrile by addition of an excess of tetraethylammonium nitrate and crystallised by slow evaporation of their methanol/acetonitrile solutions. Single-crystal X-ray measurements of **3MeCuCu**·$(NO_3^-)_4$, **6MeNiNi**·$(PF_6^-)_4$, **6MeCuNi**·$(PF_6^-)_4$, **7MeNiNi**·$(PF_6^-)_4$, **7MeCuCu**·$(PF_6^-)_4$, **7NiNi**·$(NO_3^-)_4$ and **7CuCu**·$(PF_6^-)_4$ were accomplished on a Kuma KM4CCD κ-axis diffractometer with graphite-monochromated $Mo_{K\alpha}$ radiation at 100 K (**7MeNiNi**·$(PF_6^-)_4$, **7MeCuCu**·$(PF_6^-)_4$, **7NiNi**·$(NO_3^-)_4$ and **7CuCu**·$(PF_6^-)_4$) or at 120 K (**6MeNiNi**·$(PF_6^-)_4$ and **6MeCuNi**·$(PF_6^-)_4$). The single crystals were positioned 65 mm from the KM4CCD camera. 1204 frames were measured at 1.0° intervals with counting times of 20 s (**6MeCuNi**·$(PF_6^-)_4$, **7MeCuCu**·$(PF_6^-)_4$ and **7CuCu**·$(PF_6^-)_4$), 23 s (**7MeNiNi**·$(PF_6^-)_4$), 25 s (**7NiNi**·$(NO_3^-)_4$) or 30 s (**6MeNiNi**·$(PF_6^-)_4$ and **3MeCuCu**·$(NO_3^-)_4$). The data were corrected for Lorentz and polarisation effects. A numerical absorption correction was applied. Data collection, cell refinement and data reduction were carried out with the Kuma diffraction programs CrysAlis CCD and CrysAlis RED.[11]

The structures were solved by direct methods[12] and refined by using the SHELXL program.[13,14] The refinement was based on $F^2$ for all reflections except those with very negative $F^2$ values. Weighted *R* factors, *wR*, and all goodness-of-fit, *S*, values are based on $F^2$. Conventional *R* factors are based on *F* with *F* set to zero for negative $F^2$ values. The $F_0^2 > 2\geqq(F_0^2)$ criterion was used only for calculating *R* factors and is not relevant to the choice of reflections for the refinement. The *R* factors based on $F^2$ are about twice as large as those based on *F*. Most of the hydrogen atoms were located in idealised averaged geometrical positions. In the case of **7NiNi**·$(NO_3^-)_4$, all non-hydrogen atoms, except nickel atoms, were refined isotropically because of poor diffraction. Additionally, we failed to find water hydrogen atoms. Scattering factors were taken from Tables 6.1.1.4 and 4.2.4.2 in reference [15].

CCDC-276630–276636 (for **3MeCuCu**·$(NO_3^-)_4$, **7CuCu**·$(PF_6^-)_4$, **7MeCuCu**·$(PF_6^-)_4$, **6MeCuNi**·$(PF_6^-)_4$, **7NiNi**·$(NO_3^-)_4$, **6MeNiNi**·$(PF_6^-)_4$ and **7MeNiNi**·$(PF_6^-)_4$, respectively) contain the supplementary crystallographic data for this paper. These data can be obtained free of charge from the Cambridge Crystallographic Data Centre via www.ccdc.cam.ac.uk/data_request/cif.

Details of data collection and refinement for all structures are defined in Table 1.

**Voltammetry**: Linear-scan, differential-pulse and square-wave voltammetry experiments were done by using the Autolab potentiostat (ECO Chemie, Netherlands) in a three-electrode arrangement with a silver/silver chloride (Ag/AgCl) electrode as the reference, platinum foil as the counter electrode and a glassy carbon electrode (GCE, BAS, 3 mm diameter) as the working electrode. The reference electrode was separated from the working solution by an electrolytic bridge filled with 0.1 M tetrabutylammonium hexafluorophosphate/acetonitrile (TBAHFP/AN) solution. The reference electrode potential was calibrated by using the ferrocene oxidation process in the same TBAHFP/AN solution. Acetonitrile containing 0.1 M TBAHFP was used as the supporting electrolyte solution. Argon was used to deaerate the solution and an argon blanket was maintained over the solution during the experiments.

**NMR measurements**: The NMR spectra were obtained on Varian Mercury 400, Varian Gemini 2000BB and Bruker DRX500 spectrometers. Signals are reported in ppm relative to the residual solvent signal. IR spectra (paraffin oil mulls) were recorded with a Perkin–Elmer Spectrum 2000 FT-IR spectrometer. ESI mass spectra were measured on a Mariner Perseptive Biosystem mass spectrometer. ESR spectra were registered with a Bruker ELEXYS 500 spectrometer with a nitrogen flow heater or liquid nitrogen cooler applied for measurements at higher or lower temperatures than room conditions. The spectra were taken for powder samples or samples dissolved in acetonitrile. Spectra simulations were carried out by using the XSophie software package.

  

Table 1. Details of data collection and structure refinement for all structures studied.

| Identification code | **3MeCuCu**·$(NO_3^-)_4$ | **6MeNiNi**·$(PF_6^-)_4$ | **6MeCuNi**·$(PF_6^-)_4$ | **7MeNiNi**·$(PF_6^-)_4$ | **7MeCuCu**·$(PF_6^-)_4$ | **7NiNi**·$(NO_3^-)_4$ | **7CuCu**·$(PF_6^-)_4$ |
|---|---|---|---|---|---|---|---|
| empirical formula | $C_{38}H_{58}N_{18}Cu_2O_{12}$ | $C_{44}H_{70}N_{14}Ni_2P_4F_{24}$ | $C_{44}H_{70}N_{14}CuNiP_4F_{24}$ | $C_{42}H_{76}N_{12}O_4Ni_2P_4F_{24}$ | $C_{42}H_{76}N_{12}O_4Cu_2P_4F_{24}$ | $C_{38}H_{64}N_{16}O_{12}Ni_2$ | $C_{38}H_{72}N_{12}O_6Cu_2P_4F_{24}$ |
| formula weight | 1086.10 | 1492.44 | 1497.27 | 1510.45 | 1520.11 | 1054.47 | 1500.04 |
| $T$ [K] | 100 | 120 | 120 | 100 | 100 | 100 | 100 |
| wavelength [Å$^{-1}$] | 0.71073 | 0.71073 | 0.71073 | 0.71073 | 0.71073 | 0.71073 | 0.71073 |
| crystal system | monoclinic | monoclinic | monoclinic | monoclinic | monoclinic | monoclinic | triclinic |
| space group | $P2_1/c$ | $P2_1/c$ | $P2_1/c$ | $P2_1/c$ | $P2_1/c$ | $P2_1$ | $P\bar{1}$ |
| unit-cell dimensions: | | | | | | | |
| $a$ [Å] | 12.853(3) | 8.3556(7) | 8.3408(8) | 11.556(1) | 11.6672(9) | 12.475(5) | 9.0709(8) |
| $b$ [Å] | 13.309(2) | 29.985(2) | 30.122(2) | 16.572(2) | 16.489(1) | 8.858(4) | 12.633(1) |
| $c$ [Å] | 14.176(3) | 12.379(1) | 12.3734(8) | 16.402(2) | 16.386(1) | 27.57(1) | 14.812(2) |
| $\alpha$ [°] | 90 | 90 | 90 | 90 | 90 | 90 | 102.40(1) |
| $\beta$ [°] | 107.44(2) | 105.70(1) | 105.57(1) | 94.82(1) | 93.34(1) | 99.64(3) | 93.19(1) |
| $\gamma$ [°] | 90 | 90 | 90 | 90 | 90 | 90 | 102.78(1) |
| $V$ [Å$^{-3}$] | 2313.5(7) | 2985.8(4) | 2994.7(4) | 3129.9(5) | 3146.8(4) | 3004(2) | 1607.2(3) |
| $Z$ | 2 | 2 | 2 | 2 | 2 | 2 | 1 |
| $\rho_{calcd}$ [mg m$^{-3}$] | 1.559 | 1.660 | 1.660 | 1.603 | 1.604 | 1.166 | 1.550 |
| $\mu$ [mm$^{-1}$] | 1.00 | 0.860 | 0.898 | 0.825 | 0.898 | 0.687 | 0.880 |
| $F$(000) | 1132 | 1528 | 1530 | 1552 | 1556 | 1112 | 766 |
| crystal size [mm$^{-3}$] | 0.14×0.14×0.07 | 0.53×0.08×0.08 | 0.21×0.11×0.08 | 0.21×0.11×0.09 | 0.19×0.14×0.07 | 0.22×0.11×0.10 | 0.26×0.16×0.07 |
| $\theta$ range for data collection [°] | 3.01–25.00 | 3.21–24.00 | 3.34–24.00 | 2.78–24.99 | 2.78–25.00 | 2.74–20.00 | 2.82–24.00 |
| index ranges | $-15\le h\le 15$<br>$-15\le k\le 15$<br>$-16\le l\le 16$ | $-9\le h\le 9$<br>$-34\le k\le 34$<br>$-14\le l\le 14$ | $-9\le h\le 7$<br>$-34\le k\le 34$<br>$-14\le l\le 14$ | $-13\le h\le 13$<br>$-19\le k\le 19$<br>$-19\le l\le 19$ | $-13\le h\le 13$<br>$-19\le k\le 19$<br>$-19\le l\le 19$ | $-12\le h\le 12$<br>$-8\le k\le 7$<br>$-26\le l\le 26$ | $-10\le h\le 10$<br>$-14\le k\le 14$<br>$-16\le l\le 16$ |
| reflections collected/unique | 27732/4060 | 41916/4682 | 16403/4633 | 35079/5494 | 47832/5529 | 13835/4443 | 22214/5046 |
| $R$(int) | 0.185 | 0.1204 | 0.0331 | 0.1786 | 0.0892 | 0.1552 | 0.0665 |
| absorption correction | numerical | numerical | numerical | – | numerical | – | numerical |
| max. and min. transmissions | 0.981 and 0.920 | 0.984 and 0.939 | 0.898 and 0.731 | – | 0.916 and 0.764 | – | 0.963 and 0.875 |
| refinement method | full-matrix least-squares on $F^2$ | | | | | | |
| data/restr./param. | 4060/82/310 | 4682/0/400 | 4633/0/403 | 5494/118/407 | 5529/37/489 | 4443/131/292 | 5046/172/433 |
| goodness-of-fit on $F^2$ | 1.2 | 1.117 | 1.036 | 0.975 | 1.019 | 1.284 | 0.942 |
| final $R$ indices [$I>2\sigma(I)$] | | | | | | | |
| $R1$ | 0.0914 | 0.0619 | 0.0333 | 0.0613 | 0.0481 | 0.2275 | 0.0485 |
| $wR2$ | 0.1716 | 0.1230 | 0.0787 | 0.1279 | 0.0811 | 0.4971 | 0.1013 |
| $R$ indices (all data) | | | | | | | |
| $R1$ | 0.2240 | 0.0918 | 0.0443 | 0.1358 | 0.1024 | 0.3236 | 0.0948 |
| $wR2$ | 0.2361 | 0.1376 | 0.0835 | 0.1588 | 0.0984 | 0.5738 | 0.1171 |
| absolute struct. param. | – | – | – | – | – | 0.29(12) | – |
| largest diff. peak and hole [e A$^{-3}$] | 0.96 and −0.70 | 0.38 and −0.51 | 0.37 and −0.37 | 0.98 and −0.45 | 0.48 and −0.43 | 2.31 and −0.96 | 0.83 and −0.39 |

**NMR titration experiments**: Equimolar solutions (approximately $10^{-2}$ M) of host and guest in $CD_3CN$ were prepared and mixed in NMR tubes in several different proportions. The 400 MHz $^1$H NMR spectra of pure host and guest, as well as those of mixed samples, were recorded and the association constants were obtained from fitting Equation (5) to the experimental data (see below).

## Results and Discussion

**Synthesis**: The *N*-methylated biscyclidenes were obtained by the procedure previously described for unsubstituted complexes[5,6] by using *N*,*N*′-methylated diamines and is summar-

  

ised in Scheme 1. In the case of the heterodinuclear biscyclidene **6MeCuNi**, a two-step procedure was applied.[6,7] Newly prepared materials were routinely characterised and identified by elemental analysis, ESI MS, and IR spectroscopy; diamagnetic nickel(II) complexes were also characterised by $^{13}C$ and $^{1}H$ NMR spectroscopies. The assignment of the NMR spectra was based on previously published data for similar compounds.[5,8,16]

The $^{13}C$ and $^{1}H$ NMR spectra of **7MeNiNi** are consistent with a symmetric structure of the cation. The single methyl group signal appeared at $\delta = 3.33$ ppm, which is characteristic for a *syn* position of the substituents and *lid-on*[8] configuration of the polymethylene bridge. The chemical shift of the methyl carbon atoms ($\delta = 40.9$ ppm) also confirms this geometry. The $^{13}C$ and $^{1}H$ NMR signals of cyclidene ring carbon atoms and protons are broad, thereby indicating rotation around the enamine C=C bonds that is slow on the NMR timescale. Since the number of NMR signals is larger then expected, the results indicate that the **6MeNiNi** cation in acetonitrile solution forms a mixture of slowly interconverting conformers. At higher temperatures the $^{1}H$ NMR signals become broad but no coalescence point was reached up to a temperature of 338 K. On the basis of 2D $^{1}H/^{13}C$ NMR (500/125 MHz) spectra analysis, we were able to confirm the presence in solution of three isomers in a ratio of approximately 2:1:1. The major isomer has all four methyl groups as nonequivalent and one of them occupies the *anti* position ($\delta = 3.39/49.0$ ppm), thereby leading to the *lid-off*[8] configuration of the bridge at one of the molecule corners. The remaining methyl groups absorb at $\delta = 3.36/41.1$, 3.32/40.8 and 3.31/41.0 ppm and their $^{13}C$ chemical shifts indicate the *syn* configuration. The second isomer is symmetric, with all four methyl groups occupying the *syn* position and thus giving a single methyl group signal at $\delta = 3.33/41.1$ ppm. The third, minor, isomer has two *syn* ($\delta = 3.32/41.3$ ppm) and two *anti* methyl groups ($\delta = 3.40/49.4$ ppm). This slow, on the NMR timescale, rotation around partial double C–N bonds is accompanied by rotation around exocyclic, also partially double, enamine bonds. These are the effects that contribute to the broadening of the NMR signals of the vinylic protons in the macrocycles.

**Structural details**: In general, the structures of the bismacrocycles studied are quite similar to those of previously described for **3CuNi**, **3CuCu** and **3NiNi**.[5–7] **7NiNi**·$(NO_3^-)_4$ crystallises in the $P2_1$ space group, **3MeCuCu**·$(NO_3^-)_4$, **6MeNiNi**·$(PF_6^-)_4$, **6MeCuNi**·$(PF_6^-)_4$, **7MeNiNi**·$(PF_6^-)_4$ and **7MeCuCu**·$(PF_6^-)_4$ crystallise in the $P2_1/c$ space group and **7CuCu**·$(PF_6^-)_4$ crystallises in the triclinic $P$-1 space group. With the exception of **7CuCu**·$(PF_6^-)_4$, they all crystallise in the monoclinic system. **3MeCuCu**·$(NO_3^-)_4$, **6MeNiNi**·$(PF_6^-)_4$, **6MeCuNi**·$(PF_6^-)_4$, **7MeNiNi**·$(PF_6^-)_4$, **7MeCuCu**·$(PF_6^-)_4$ and **7CuCu**·$(PF_6^-)_4$ crystallise at special positions (around the symmetry centres) and in such cases only half of the molecules are independent. Those of the molecules with labels carrying the suffix Me are methylated at the bridge nitrogen atoms.

Despite different metal ions, the bismacrocycles we study form quite similar rectangular molecules (see Figure 1). Each bismacrocycle consists of two macrocycles which close the macrocyclic cavity and are linked by aliphatic chains (three, six or seven carbon atoms long). In order to fine tune the properties in this series of bismacrocycles, we change the central metal ions ($Ni^{II}$, $Cu^{II}$), the counterions, the length of aliphatic linkers and, most importantly, we consider the role of hydrogen atoms and methyl groups at the external nitrogen atoms (N5, N6, N5A, N6A or N9 up to N12 for molecules in Figure 1).

The dimensions of cavities in particular bismacrocycles are given in Table 2 and Figure 2. In general, there are two groups of structures with slightly different $Me^{II}\cdots Me^{II}$ distances (approximately 4.1 Å for **6MeNiNi** and **6MeCuNi**, 4.37 Å for **3MeCuCu** and 7.1–7.8 Å for bismacrocycles with aliphatic linkers that are seven carbon atoms long). For comparison, the equivalent $Me^{II}\cdots Me^{II}$ distances are approximately 4.4 Å in **3CuNi** and **3CuCu**[6] and 4.5 Å in **3NiNi**. Apparently, the shorter length of the Ni···Cu contact than that for Ni···Ni can be explained by the different strengths of the interactions between the metallic centres. The second distance characterising the cavity size, that is, the separation of the aliphatic linkers, is in the range from 14.5 Å for **7CuCu** up to approximately 15.5 Å for the methylated compounds. All important interatomic distances defining details of the cavities in the bismacrocycles are given in Table 2.

We also want to stress that in almost all of the bismacrocycles the separation of the external nitrogen atoms (see Figure 2) is usually longer than the separation of the metal centres. This means that a kind of attraction must be present in the bismacrocycles between the macrocyclic fragments arranged face-to-face.

The presence of small guest molecules (these are usually disordered water molecules; Figure 3) in the cavities formed by the bismacrocycles in the solid state is one of the most important differences in relation to the previously studied bismacrocycles. This occurs in the cases of **7MeNiNi**·$(PF_6^-)_4$, **7MeCuCu**·$(PF_6^-)_4$, **7NiNi**·$(NO_3^-)_4$ and **7CuCu**·$(PF_6^-)_4$. Usually these guest molecules are located a bit off the centre of the cavities. Apparently the guest molecules are arranged in such a way as to keep hydrogen atoms involved in hydrogen-bond-type interactions with other solvent molecules in the plane, more or less parallel to the macrocyclic fragments and located close to the centre of the molecule. We were unable to locate the water hydrogen atoms directly from difference Fourier maps because of poor diffraction, even at low temperatures (100 K). Such a location of the water molecules enables interactions between the lone electron pairs of the oxygen atoms and the central metal ions. This is, in fact, a similar situation to the catenanes we reported previously.[7] The molecules with aliphatic linkers that are six carbon atoms long do not host any solvent molecules.

Positively charged bismacrocyclic cations are surrounded by negatively charged counterions and water molecules. This is well illustrated in Figure 3. The counter moieties surround the bismacrocycles in a symmetric way, thereby creat-

  

Table 2. The most important structural parameters defining cavity sizes in bismacrocycles. Plane1 and plane2 are least-squares planes based on nitrogen atoms and metal ions located in the face-to-face stacked macrocycle. All distances in Å (see Figure 2).

| Compound | M1···M2 | M2···Plane1 | M1···Plane2 | C15···C15$1 or C25···C34[a] | N5···N6 N9···N10 N11···N12 | C12···C18 C22···C28 C31···C37 C12···C17 |
|---|---|---|---|---|---|---|
| **3MeCuCu**·$(NO_3^-)_4$ | 4.366(2) | 3.912(6) | – | 15.14(1) | 3.17(4) | 2.61(5) |
| **6MeNiNi**·$(PF_6^-)_4$ | 4.156(1) | 4.080(1) | – | 15.37(1) | 5.148(6) | 5.296(7) |
| **6MeCuNi**·$(PF_6^-)_4$ | 4.071(1) | 3.98(2) | – | 15.410(5) | 5.123(3) | 5.282(4) |
| **7MeNiNi**·$(PF_6^-)_4$ | 7.277(2) | 7.225(3) | – | 15.45(1) | 7.819(6) | 7.653(8) |
| **7MeCuCu**·$(PF_6^-)_4$ | 7.176(1) | 7.092(2) | – | 15.466(8) | 7.829(4) | 7.644(5) |
| **7NiNi**·$(NO_3^-)_4$ | 7.060(8) | 7.07(1) | 7.13(1) | 14.99(5) | 7.69(4) 7.72(5) | 7.47(6) 7.38(6) |
| **7CuCu**·$(PF_6^-)_4$ | 7.752(1) | 6.727(6) | – | 14.45(1) 14.79(4) | 7.502(6) | 7.066(8) |

[a] C25···C34 for **7NiNi**·$(NO_3^-)_4$.

ing a pseudosymmetric environment and forming quite a number of hydrogen-bond-type close contacts. Both the bismacrocyclic cations and anions also interact with some water molecules located in the close neighbourhood outside the bismacrocyclic cavities. The distribution of the guest moieties in the bismacrocyclic cavities and the closest counterions in all of the bismacrocycles studied is shown in Figure 1S in the Supporting Information.

From the point of view of the 3D arrangement of molecules, one can differentiate two types of arrangement (Figure 4). Let us first define the long axis of a bismacrocyclic moiety as more or less parallel to the CC line defining the longer cavity size (also parallel to the macrocyclic planes). For the first class of structures, such axes characterising the neighbouring moieties in the crystal lattice form an angle other than 180°. In the second type of structure, this angle is equal to 180°. For both classes of structures, the bismacrocyclic cations fill the voids created by neighbouring molecules. An additional factor influencing the formation of the 3D structures is the strong electrostatic interactions with anions. For packing of the molecules in all of the crystals studied, see Figure 2S in the Supporting Information.

As far as the geometry of the bismacrocyclic moieties is concerned, it appears that most of the bond lengths in bismacrocycles have typical bond-length values. The Cu–N bonds are approximately 0.05 Å longer than the Ni–N ones (1.92 and 1.86 Å, respectively; see Table 1S in the Supporting Information). There are four CH–NH–$CH_2$ groups in the bismacrocycles unless the moieties occupy some special positions. The two CH–NH–$CH_2$ groups linked with the same macrocycle are located *cis* relative to each other, whereas when the CH–NH–$CH_2$ groups are linked by the aliphatic linkers, $(CH_2)_6$ or $(CH_2)_7$, their relative location is *trans* (see Figure 2). In general, there can be *cis* or *trans* isomerism both on the macrocyclic units and on the ends of the aliphatic linkers.

It appears that the electron density of the exocyclic nitrogen atoms is conjugated with the delocalised electron density of the macrocyclic ring. In consequence, the N–C and C–C bonds linking these nitrogen atoms with the macrocyclic ring have intermediary character between single and double bonds. A closer inspection of the numerical values reveals that the formally double bonds have bond lengths closer to single bonds whereas the formally single bonds are quite short and similar to the C=N bonds.

When one replaces the NH hydrogen atoms with methyl groups, the geometric structure of the bismacrocycles is not much changed. However, a closer inspection of structural data shows that, because of the strain caused by the short contacts between the methyl and the closest C–H groups of the macrocyclic moieties, the CH–NMe–$CH_2$ fragment is less planar than in the case of the nonmethylated compounds. This is confirmed by increasing values of proper torsion angles, such as C1–C10–C11–N and similar angles (see Table 1S in the Supporting Information). These angles are 2–3 times larger (approximately 12–18°) for the methylated derivatives than for the nonmethylated ones (approximately 6°). As a consequence of steric strain in the methylated species, increasing nonplanarity of the macrocyclic units is also observed. When the least-squares best planes based on the nitrogen atoms and the metal ion are defined, it appears that, for the bismacrocycles with aliphatic linkers that are 7 carbon atoms long, the deviation of the nitrogen atoms is approximately 0.12 Å for the methylated macrocyclic fragments and approximately 0.02 Å for the nonmethylated ones. In the case of bismacrocycles with shorter carbon linkers, the planarity of the central bismacrocyclic fragments is comparable to the planarity of the nonmethylated fragments. This could be due to increasing face-to-face interactions in such systems. Additionally, in the case of the methylated bismacrocycles, slightly shorter Me–N bond lengths are present although the whole central part of the macrocyclic moieties is less planar. This is possible due to a decreasing conjugation of flexible electron density in both the CH–NMe–$CH_2$ and bismacrocyclic fragments. All such arguments based on structural data support a conclusion that such subtle changes in electron-density distribution of the macrocyclic fragments affect the interactions of the bismacrocycles; an increase in the amount of electron density increases interactions between the macrocyclic units, thereby decreasing the $Me^{II}\cdots Me^{II}$ separation. This seems to be a convenient way of fine-tuning of the properties of bismacrocycles.

**Electrochemistry**: When the spacer length between the $Cu^{II}$ and $Ni^{II}$ in bismacrocyclic complexes is decreased from $n=7$ to $n=3$ (Table 3), the formal potentials are displaced to more positive values. This can be interpreted in terms of increasing electrostatic repulsion between the centres. Methyl-

  

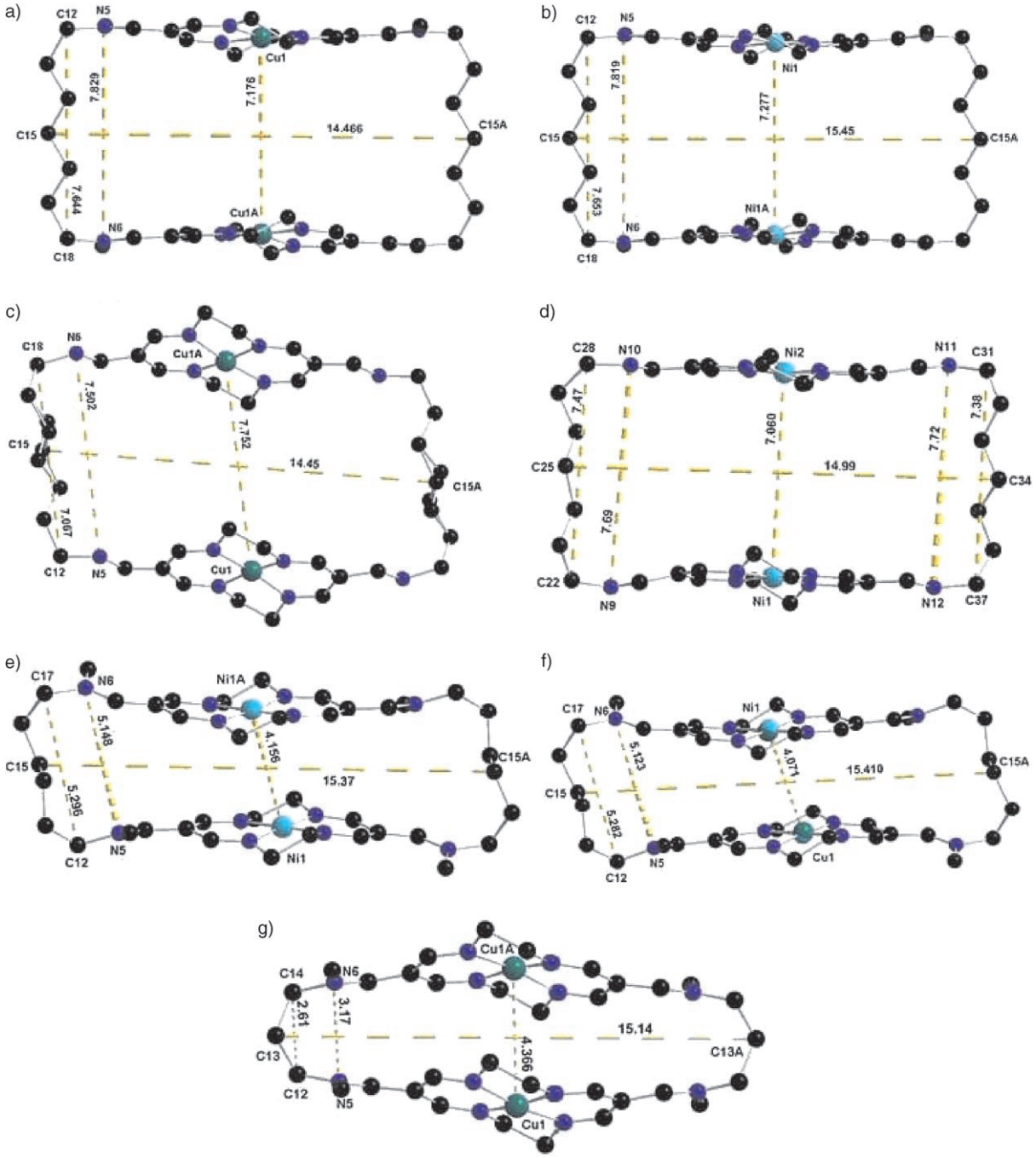


Figure 2. Definition of the most important interatomic distances in a) **7MeCuCu**·$(PF_6^-)_4$, b) **7MeNiNi**·$(PF_6^-)_4$, c) **7CuCu**·$(PF_6^-)_4$, d) **7NiNi**·$(NO_3^-)_4$, e) **6MeNiNi**·$(PF_6^-)_4$, f) **6MeCuNi**·$(PF_6^-)_4$, g) **3MeCuCu**·$(NO_3^-)_4$. Color code: C: black; N: blue; Cu: dark green; Ni: turquoise.

ation does not change the direction of changes; however, a shift of each of the methylated forms towards negative potentials clearly shows increasing donor abilities of the compounds (Figure 5). Figure 6 reveals a splitting of the voltammetric peaks observed for **6MeNiNi** into two, a result indicating stabilisation of the intermediate mixed-valence state as compared to the longest bridge analogues where no splitting is observed (Figure 7). The stability of the mixed-valence complex is exhibited by the extent of splitting of the formal potentials and can be observed either by electrochemistry or by the appearance of an intervalence-transfer absorption band, as previously reported for the near-infrared region with some other intervalent compounds. The splitting is seen for $Ni^{II}$ complexes, while only some widening of the peak is detected for the corresponding $Cu^{II}$ systems.

The redox characteristics of the macrocyclic complexes are presented in Table 3. The electrooxidation process for the $Ni^{II}$ complex corresponds to the scheme shown in Equation (1).

  

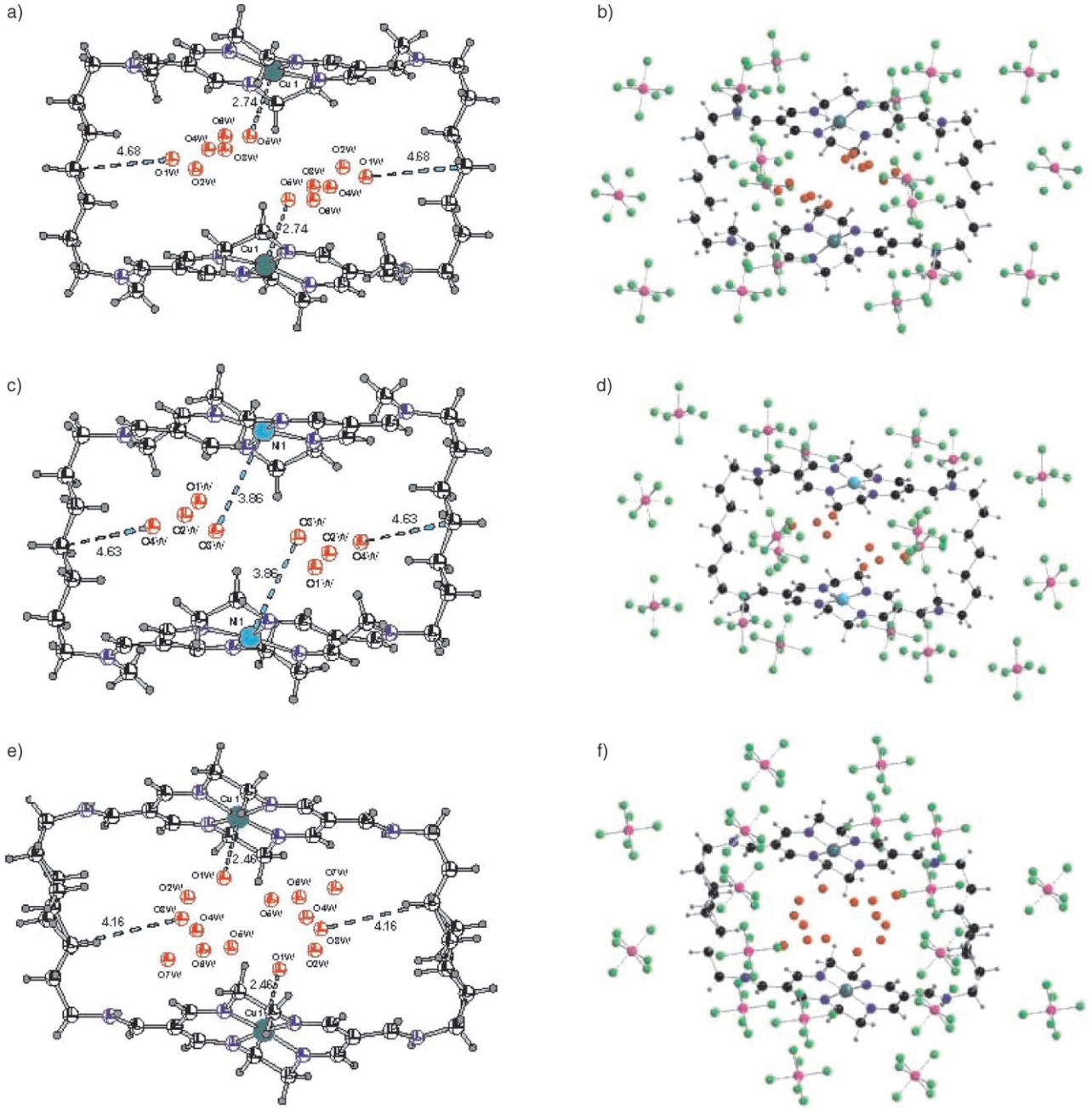


Figure 3. Distribution of the guest moieties in the bismacrocyclic cavities and the closest counterions in: a) and b) **7MeCuCu**·$(PF_6^-)_4$, c) and d) **7MeNiNi**·$(PF_6^-)_4$, e) and f) **7CuCu**·$(PF_6^-)_4$.

$$Ni^{II}Ni^{II} - e \xrightarrow{E_1} Ni^{II}Ni^{III} - e \xrightarrow{E_2} Ni^{III}Ni^{III} \quad (1)$$

An additional equilibrium is the disproportionation of the $Ni^{II}Ni^{III}$ complex affecting the shape of the voltammogram, as described by Equation (2), where $K_{com} = \exp[(\Delta E^o)F/RT]$ and $\Delta E_o$ is the standard potential difference between the successive monoelectron transfers.

$$Ni^{II}Ni^{III} \overset{K_{com}}{\rightleftharpoons} Ni^{II}Ni^{II} + Ni^{III}Ni^{III} \quad (2)$$

For $K_{com} < 4$, $E_1 - E_2 < 35.6$ mV and the mixed-valence form is unstable.[17,18] When $K_{com}$ is equal to 4, the centres are noninteractive, while larger values of $K_{com}$ indicate interaction between the redox centres.

Table 3 depicts all of the comproportionation constants. The behaviour of **6MeCuCu** and **6MeNiNi** and **6MeCuNi** (Figure 6) is in line with crystallographic results (the shorter intermetallic distance observed in the solid state is probably preserved in solution).

  

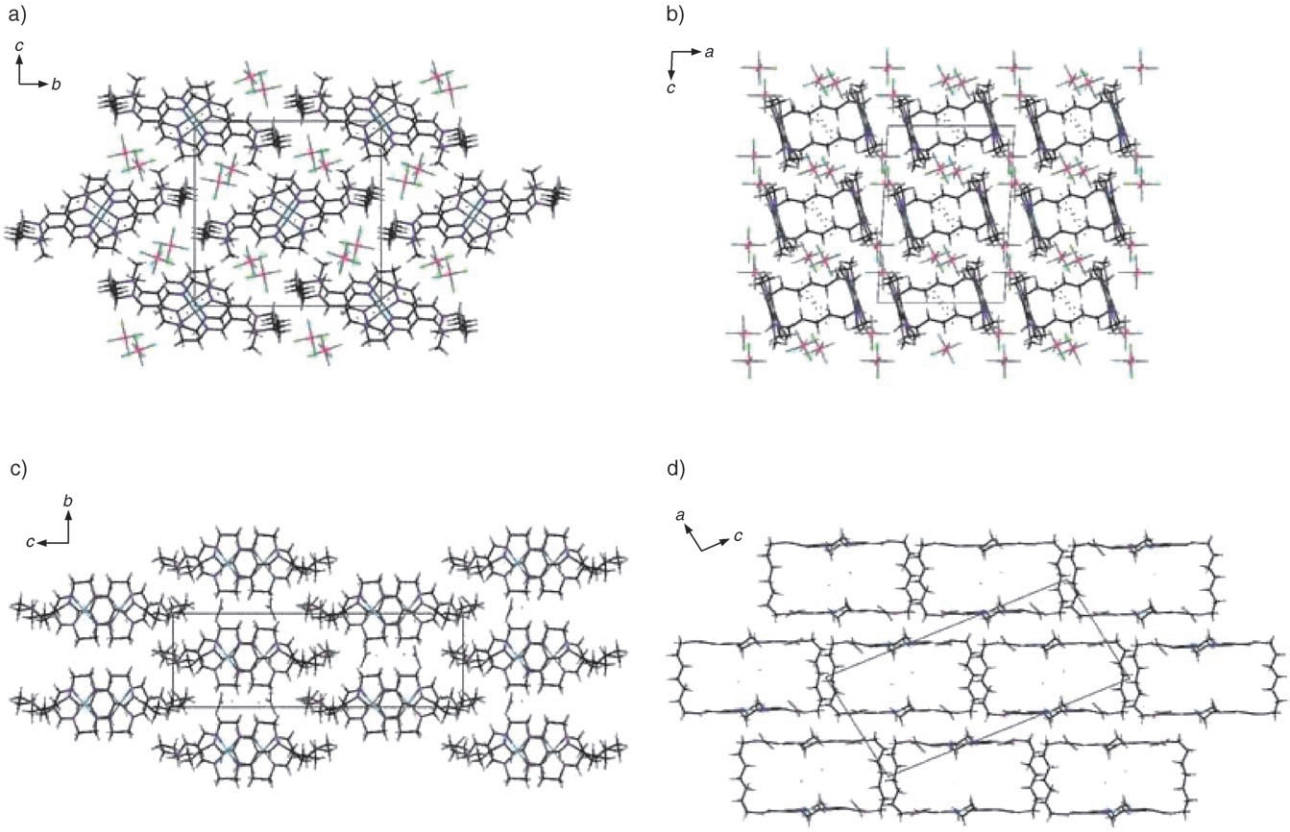


Figure 4. Examples of typical packing modes and 3D crystal structures for the compounds studied: a) and b) **7MeCuCu**·$(PF_6^-)_4$, c) and d) **7CuCu**·$(PF_6^-)_4$. a,c) View along the *x* axis; b,d) view along the *y* axis. For packing of molecules in all crystals, see Figure 2S in the Supporting Information. Color code: C: black; H: grey; N: blue; O: red; Cu: dark green; P: pink; F: light green; Ni: turquoise.

Table 3. Comparison of the redox properties of homo- and heterodinuclear complexes.

| Compound | $E^{o\prime}_{Cu}$ [V] | $E^{o\prime}_{Ni}$ [V] | $E^{o\prime}_{Ni}-E^{o\prime}_{Ni}$ [a] | $K_{com}$ |
|---|---|---|---|---|
| **7CuCu** | 1.052 | | | 4.5 |
| **7MeCuCu** | 0.980 | | | – |
| **7NiNi** | | 1.326 | 0.274 | 15.9 |
| **7MeNiNi** | | 1.272 | | – |
| **3CuCu** | 1.243 | | | 3.8 |
| **3MeCuCu** | 1.103 | | | – |
| **6MeCuCu** | 0.974 | | | – |
| **6MeNiNi** | | 1.184[b] | | 20.1 |
| | | 1.295[b] | | – |
| **6MeCuNi** | 1.001 | | 0.332 | |
| | | 1.333 | | |
| | | 1.390 | | |

[a] The difference between formal potentials of nickel and copper centres for hetero- and homodinuclear complexes. [b] Ni signals split into two for the dinickel complex with the shortest linkers, **6MeNiNi**.

Insertion of methyl groups into all bismacrocycles leads to a shift of oxidation by several tens of mV towards more negative potentials, a result indicating an improvement in the donor abilities of the complexes. This strengthening of donor properties will affect binding properties of these compounds towards π-donor guests, as will be shown below.

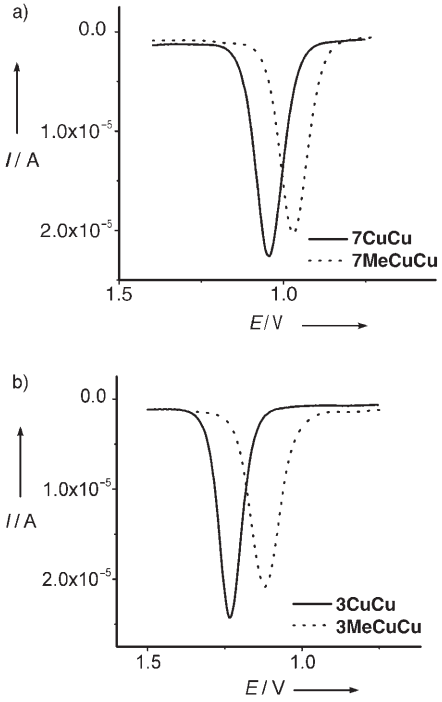


Figure 5. Differential pulse voltammograms for 1 mM $Cu^{II}$ bismacrocyclic complexes recorded by using GCE in 1 M TBAHFP/AN solution: a) **7CuCu** and **7MeCuCu**, b) **3CuCu** and **3MeCuCu**. Pulse amplitude: 0.025 V.

  

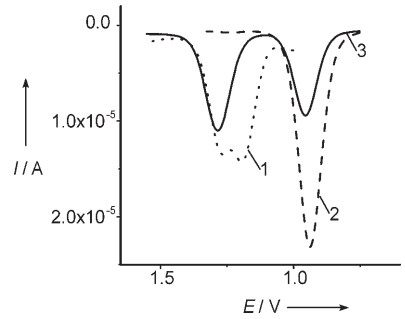


Figure 6. Differential pulse voltammograms for 1 mM dinuclear complexes recorded by using GCE in 1 M TBAHFP/AN solution: 1) **6MeNiNi**, 2) **6MeCuCu**, 3) **6MeCuNi**. Pulse amplitude: 0.025 V.

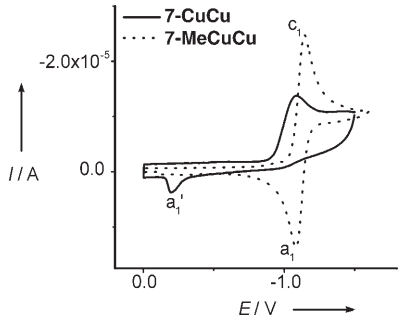


Figure 8. Cyclic voltammograms for 1 mM $Cu^{II}$ bismacrocyclic complexes **7CuCu** and **7MeCuCu** recorded by using GCE in 1 M TBAHFP/AN solutions. $v = 0.05\ V\,s^{-1}$.

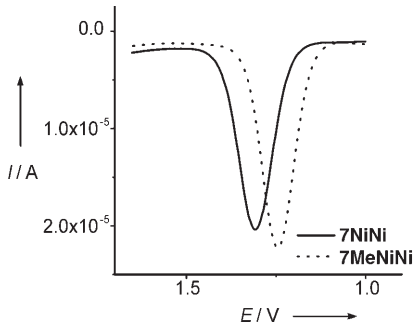


Figure 7. Differential pulse voltammograms for methylated and nonmethylated 1 mM $Ni^{II}$ dinuclear complexes recorded by using GCE in 1 M TBAHFP/AN solution. Pulse amplitude: 0.025 V.

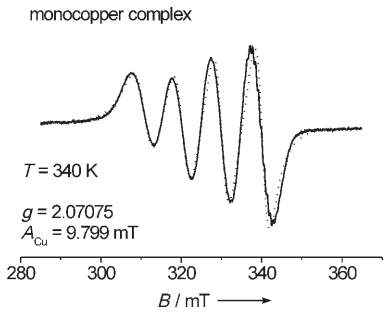


Figure 9. Isotropic ESR spectrum of the **6MeCuNi** in acetonitrile solution. Dotted line = simulated spectrum.

**Stabilisation of low-oxidation states by methylation**: In the case of the methylated **7MeCuCu**, a reversible reduction of copper(II) to copper(I) at the potential −1.14 V is observed (Figure 8, peaks $c_1/a_1$). In the corresponding nonmethylated complex, the copper(I) form was not stable and the copper metal was deposited on the electrode surface. Its oxidation peak, $a_1'$, can be resolved in the voltammogram. The increase of copper(I)-complex stability upon methylation may be attributed to a change in the structure of the complex, thereby allowing tetrahedral deformation to be achieved more easily in the presence of methyl groups.

**ESR spectroscopy**: The ESR spectra were registered for the bismacrocyclic complexes with one nickel and one copper ions (**6MeCuNi)** or two copper ions (**6MeCuCu** and **7MeCuCu**; Figures 9–12). For the **6MeCuNi** compound, the observed four peak structure of the ESR spectrum is typical for planar complexes with one paramagnetic copper(II) centre (Figure 9). **6MeCuNi** dissolved in acetonitrile exhibits four hyperfine signals coming from the interaction between the paramagnetic copper nucleus with the nuclear spin $I = {}^3/_2$ and the unpaired electron residing on the $d_{x^2-y^2}$ orbital. For the simulated spectrum fitted to the experimental one, the $g$ factor and the hyperfine coupling constant $A_{Cu}$ obtained are equal to 2.07075 and 9.799 mT, respectively. This interaction is included in the spin hamiltonian $\mathscr{H}$. The energy of the electronic levels in the magnetic field is described by Equation (3),[19] where $\beta$, $g$ and $\boldsymbol{B}$ are the Bohr magneton, electron Zeeman factor and external magnetic field, respectively, $\boldsymbol{S}$ and $\boldsymbol{I}$ are the electron- and nuclear-spin operators for the copper ion, $\boldsymbol{S}_i$ and $\boldsymbol{I}_i$ are spin operators for the nitrogen and hydrogen atoms in the closest neighbourhood, and $A_{Cu}$, $A_N$ and $A_H$ are the hyperfine and superhyperfine coefficients for copper, nitrogen and hydrogen atoms.

$$\mathscr{H} = \beta g \boldsymbol{B}\cdot\boldsymbol{S} + A_{Cu}\boldsymbol{I}\cdot\boldsymbol{S} + \sum_{i=1}^{4} A_{Ni}\cdot\boldsymbol{I}_i\cdot\boldsymbol{S}_i + \sum_{i=1}^{4} A_{Hi}\cdot\boldsymbol{I}_i\cdot\boldsymbol{S}_i \quad (3)$$

When the sample is diluted, the peak of the nuclear magnetic number $M_I = -{}^3/_2$ is split and shows the superhyperfine structure. The splitting is caused by four coordinating nitrogen atoms and some of the hydrogen atoms situated in closest vicinity of the copper centre.[18b] Four nitrogen atoms are seen by ESR spectroscopy as equivalent and—having nuclear spin $I = 1$—split the electronic level into nine. Thus, nine peaks should be observed with relative intensities calculated from the Pascal triangle as 1:4:10:16:19:16:10:4:1. The measured superhyperfine coefficient is $A_N = 1.44$ mT. There is an additional signal in the spectrum between two peaks related to the nitrogen atoms; this signal is probably due to hydrogen atoms located next to the paramagnetic centres. There are two groups of equivalent hydrogen paramagnetic nuclei, H′ and H″ in the vicinity of the unpaired copper electron. Both of the groups are separated by three molecular bonds (Scheme 2). The four H′ hydrogen atoms of the azomethine

  

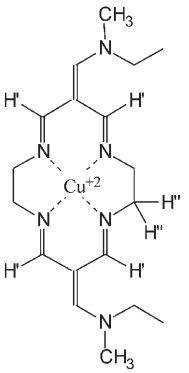


Scheme 2. Structures of cyclidene macrocyclic fragment.

moieties affect the spectrum more than the eight H″ hydrogen atoms of the diiminoethane bridges. The nuclear spins of the H′ atoms are transmitted through σ bonds created by $sp^2$-hybridised orbitals of the carbon and nitrogen atoms rather then the $sp^3$ ones. The repetitive splitting from four equivalent H′ hydrogen nuclei multiplies each of the nitrogen signals into five with relative intensities of 1:4:6:4:1. The superhyperfine coefficient $A_H$ for hydrogen appears to be $A_H = {}^1/_2 \times A_N = 0.7$ mT. For the simulated ESR spectrum, the relative intensities of the 21 signals are 1:4:10:20:35:56:80:104:125:140:146:140:125:104:80:56:35:20:10:4:1. The experimental spectrum contains only 15 features (Figure 10). Six signals are missing because of their low intensities. This superhyperfine structure points to the very stable magnetic surrounding of the copper ion in **6MeCuNi**.

The sample dissolved in acetonitrile and cooled down to 125 K, below the freezing point of the solvent ($T = 227$ K), shows the ESR anisotropic copper spectrum of the glassy state. In the spectrum (Figure 11), three of the four peaks (I, II, IV) reflect the electron–copper-nucleus coupling. They are related to the $Z$ direction perpendicular to the coordination plane. The remaining signals related to the $x$ and $y$ axis are overlapped and form one bulky peak. The simulation of this spectrum gives $g_z = 2.144$, $A_z = 21.2$ mT and $g_x = g_y = 2.037$, $A_x = A_y = 2.2$ mT. The calculated averaged values of these parameters are $g = 2.073$ and $A_{Cu} = 8.53$ mT. The $g$ factor is identical to that obtained from the isotropic solution, whereas the copper hyperfine constant $A_{Cu}$ is different. The difference can be explained by the poor reliability of the $g$ and $A$ factors in the $x$ and $y$ directions. The spectrum taken for a powdered sample exhibits the one broad illegible signal that is common for concentrated copper compounds because of the exchange narrowing effect.[18a]

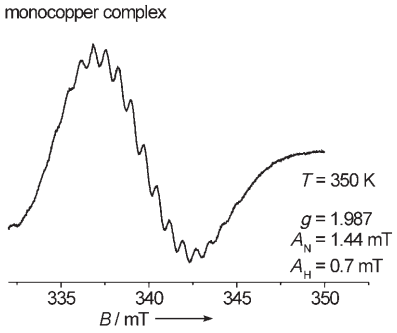


Figure 10. Superhyperfine structure of the ESR peak with $M_I = -{}^3/_2$ in the isotropic spectrum of **6MeCuNi** in acetonitrile solution.

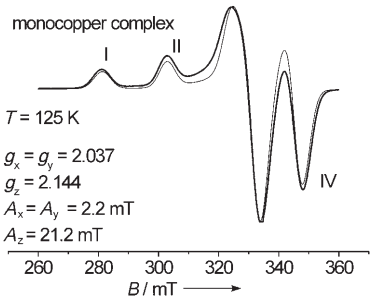


Figure 11. Glassy-state ESR spectrum of **6MeCuNi** in acetonitrile solution. Dotted line = simulated spectrum.

For the **6MeCuCu** bismacrocycle containing two copper ions, the ESR spectrum is different from that obtained for **6MeCuNi**. The spectrum displays seven instead of four peaks. With increasing temperature, the spectra become better defined (Figure 12a). The separation of signals is exactly two times smaller than the $A_{Cu}$ value for the monocopper complex. The set of signals reflects the interactions between the two copper ions. The two unpaired electrons with $S = {}^1/_2$ and surrounding copper nuclei with $I = {}^3/_2$ form coupled electronic levels. Their energies can be described in the external magnetic field by the spin Hamiltonian, $\mathscr{H}$, described by Equation (4),[18a] where $\boldsymbol{S}_1$, $\boldsymbol{S}_2$ and $\boldsymbol{I}_1$, $\boldsymbol{I}_2$ are electron- and nuclear-spin operators for the two copper ions and $J$ is the electron-exchange coupling constant.

$$\mathscr{H} = \beta g \boldsymbol{B} \cdot (\boldsymbol{S}_1 + \boldsymbol{S}_2) + A_{Cu}(\boldsymbol{I}_1 \cdot \boldsymbol{S}_1 + \boldsymbol{I}_2 \cdot \boldsymbol{S}_2) + J\boldsymbol{S}_1 \cdot \boldsymbol{S}_2 \qquad (4)$$

It is accompanied by an effective nuclear spin number of $\boldsymbol{I} = 3$. This gives seven peaks separated on the magnetic-field scale by ${}^1/_2 A_{Cu}$. The relative intensities of these signals should be 1:2:3:4:3:2:1. The observed intensities are not in accord with this rule. The peaks at the positions of the single copper signals are stronger than the other ones. A plausible explanation is that a fraction of the molecules can host some solvent guests in the solution. The molecules of solvent decrease the Cu···Cu magnetic interactions, as was observed in the case of catenanes.[7] For the rest of the molecules, the magnetic interactions seem to be present.

The electron coupling can be transmitted through hybridised σ electron bonds containing enough contribution of the s orbitals. In terms of topology this transmission ranges up to three–five bonds. In the described case, the copper ions are topologically separated by more than five bonds, so interaction between them is rather unlikely. The only possibility could be a direct through-space interaction between the copper ions, which are in close contact. This is confirmed by X-ray studies of **6MeCuCu**, which has a short Cu···Cu distance. Also, the electrochemical data point to in-

  

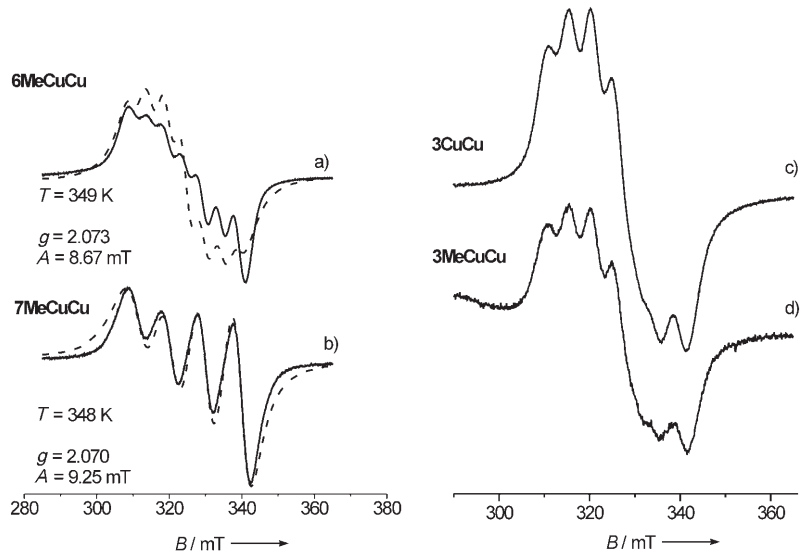


Figure 12. Isotropic and simulated (dotted line) ESR spectra of the dicopper bismacrocycles in acetonitrile solution: a) **6MeCuCu**, b) **7MeCuCu**, c) **3CuCu** and d) **3MeCuCu**.

teractions between metallic ions in the bismacrocyclic complexes with aliphatic chains that are six carbon atoms long. In such conditions, two unpaired electrons of the copper ions form some new coupled electronic states with $S=1$ or 0. At room temperature, the triplet state is populated and the ESR transitions between its levels are visible. However, the dissolved sample does not give the signal in the half-field region. At low temperature (about 140 K), the frozen sample exhibits one broad signal without any details.

Two similar ESR spectra with multiplied hyperfine lines were registered for **3CuCu** and **3MeCuCu**, which have the shortest separating alkyl chains (Figure 12a, d). However, the ESR lines are not so distinctive in comparison to the complex with linking chains of six carbon atoms. The blurring of the spectra can be caused by a larger contribution of the exchange narrowing effect, which gives one broad line and overlaps the spectrum. The effect is stronger when the paramagnetic entities (copper ions) are more concentrated, as is the case for molecules with shorter alkyl chains. Moreover, the distance between the copper ions in the molecules of the **3CuCu** and **3MeCuCu** complexes is slightly larger and it is not as well defined as in the **6MeCuCu** complex. The differences in these distances can result in a less intense spectrum that reflects the exchange coupling.

When the bridging moiety is elongated to the heptyl chain in the dicopper complex (**7MeCuCu**), the distance between the copper ions becomes too large and the spin–spin coupling is not detected by ESR spectroscopy (Figure 12b). Only a typical hyperfine structure with four peaks related to the interaction of the copper electron with its nucleus is observed. It confirms the previous supposition that the coupling between two copper electrons is transmitted through space. In this case, the superhyperfine structure from nitrogen and hydrogen atoms was not found. This suggests that there is some magnetic interaction between the copper centres in the dicopper complexes that is smearing the superhyperfine splitting.

**Host–guest interactions**: The cyclisation reaction between 1,7-diaminoheptane and *O*-methylated[14] cyclidene complexes **1Cu** or **1Ni** carried out in the presence of dibenzo-24-crown-8 has led to the self-assembly of the respective catenanes. Their structures are based on donor–acceptor interactions between the π-electron-rich aromatic rings and π-electron-deficient cyclidene units. The same type of interactions should result in the affinity of the bismacrocyclic receptors towards selected electron-rich guests, benzene and naphthalene derivatives (**A** and **B**, respectively; Scheme 3) and tetrathiafulvalene (**C**). The $^1$H NMR spectra of mixtures of aromatic guests and dinickel bismacrocyclic complexes linked with three, five[5] and six carbon atom chains gave a

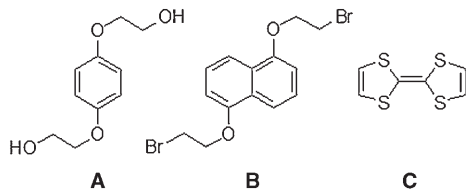


Scheme 3. Selected electron-rich guests: benzene derivative (**A**), naphthalene derivative (**B**) and tetrathiafulvalene (**C**).

simple sum of the spectra of the mixture components. On the other hand, the spectra of **7NiNi** and **7MeNiNi** showed substantial changes of the proton resonance frequencies relative to the spectra of pure components (Figure 13), a result indicating binding of the guest molecules by the bismacrocyclic hosts.

The $^1$H NMR signals of aromatic guests were also substantially broadened in the presence of paramagnetic **7CuCu** and **7MeCuCu** host complexes (Figure 14). Since such broadening was not observed in the case of dicopper receptors with smaller cavities (**3MeCuCu**), this result confirms the formation of the host–guest complexes.

The stoichiometry of the host–guest complexes was established by the Job's method of continuous variations.[18]

The Job's plots for the studied systems are shown in Figure 15. The complexation-induced shift of the $^1$H NMR resonance for the guest moiety is shown as a function of the host mole fraction while the total concentrations are kept constant. In all cases, 1:1 stoichiometry was found.

The association constants were determined by $^1$H NMR titration ($[D_3]CH_3CN$ solution) from the dependencies of the

  

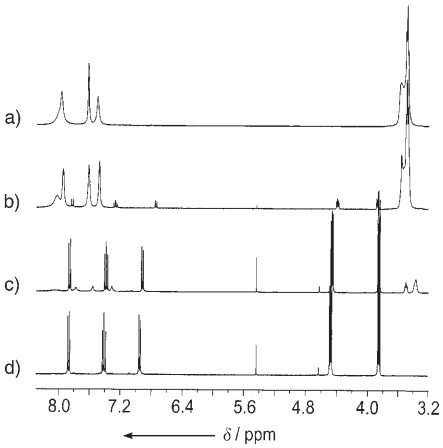


Figure 13. Partial $^1$H NMR (400 MHz, $CD_3CN$) spectra of a) host **7NiNi**, d) guest **2** and host–guest mixtures in a ratio of b) 10:1 and c) 1:10.

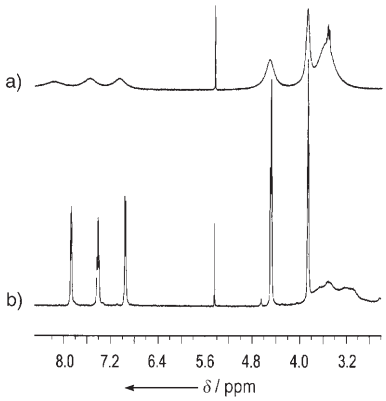


Figure 14. Partial $^1$H NMR (400 MHz, $CD_3CN$) spectra of the host–guest mixtures in a 1:1 ratio of a) **7MeCuCu** and guest **2**, b) **3MeCuCu** and guest **2**.

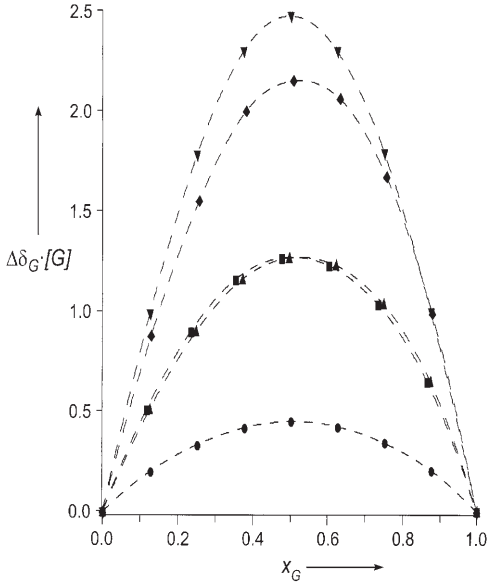


Figure 15. Job's plots for the systems containing bismacrocyclic host **7NiNi** and guest **A** (▲), host **7NiNi** and guest **B** (◆), host **7MeNiNi** and guest **A** (●), host **7MeNiNi** and guest **B** (■) and host **7NiNi** and guest **C** (▼).

proton resonance frequencies of the guest molecules on the ratio of the host/guest concentrations. The association constants, $K_{assoc}$, were obtained from simultaneous fits of Equation (5) to the experimental data with the assumption that the observed frequencies are the molar-fraction-weighted averages of the respective frequencies in the free guest molecules and those for the host–guest complexes.

$$\delta^G_{obs}(i,n) = \frac{[G]^n_0+[H]^n_0+\frac{1}{K_{assoc}}-\sqrt{([G]^n_0+[H]^n_0+\frac{1}{K_{assoc}})^2-4[G]^n_0[H]^n_0}}{2[G]^n_0}\cdot\delta^G_{max} \quad (5)$$

where

$$K_{assoc}=\frac{[GH]}{[G][H]}$$

$$\delta^G_{obs}(i,n)=\overline{\delta^G_{obs}}(i,n)-\delta^G_{obs_i}=x_{GH}(\delta^{GH}_i-\delta^G_i)$$

where

$$\delta^{GH}_i-\delta^G_i=\delta^G_{max_i}$$

In Equation (5), $[G]$ is a concentration of the guest moiety, $[H]$ stands for the host moiety concentration, $[GH]$ is a host–guest associate concentration and $\delta_i$ is the chemical shift of the $i$-th proton.

For each such fit, the variable parameter set included the $K_{assoc}$ values and the values of $\Delta\delta_{0i}$ ($i=1,2\ldots n$, where $n$ is the number of signals monitored). The values of the association constants, $K_{assoc}$, are collected in Table 4.

Table 4. Association constants, $K_{assoc}$ [$M^{-1}$] for 1:1 host–guest complexes.

| Host | Guest | $K_{assoc}$ | log $K_{assoc}$ |
|---|---|---|---|
| **7NiNi** | **A** | 91 ± 18 | 1.96 |
| **7NiNi** | **B** | 198 ± 28 | 2.30 |
| **7NiNi** | **C** | 221 ± 3 | 2.34 |
| **7MeNiNi** | **A** | 62 ± 7 | 1.79 |
| **7MeNiNi** | **B** | 123 ± 19 | 2.09 |

It appears that the methylated receptors bind the π-donor guests more weakly then the nonmethylated ones. On the other hand, larger donors (naphthalene derivatives) have higher affinity towards both the **7NiNi** and **7MeNiNi** bismacrocycles. These observations confirm the donor–acceptor nature of these host–guest interactions.

## Conclusion

New face-to-face *N*-methylated biscyclidene complexes have been synthesised and characterised. They form rectangular box-like cations enclosing an empty space inside. These moi-

  

eties are surrounded in the solid state by a shell of counterions. It appears that, in the case of sufficiently large intramolecular voids, for example, with aliphatic linkers that are seven carbon atoms long, they can host some small guest molecules such as water or π-electron-donating compounds. For the *N*-methylated species, the exocyclic iminomethylidene groups are slightly out of the macrocycle plane and some larger deviations from planarity are observed. This increasing steric strain is associated with the flow of electron density towards the central metal cations.

For the bismacrocyclic dinuclear complexes containing two nickel or two copper ions, the intramolecular interactions between the metallic centres are strengthened through methylation of the macrocyclic components relative to the nonmethylated species.

When the spacer length in the $Cu^{II}$ and $Ni^{II}$ bismacrocyclic complexes is decreased from $n=7$ to $n=3$, the formal potentials are shifted to more positive values. This can be interpreted in terms of increasing electrostatic repulsion between the centres. Methylation does not alter the direction of the changes; however, less positive values of formal potentials point to better donor abilities of the methylated derivatives. Splitting of the voltammetric peaks into two is observed for the Ni bismacrocycle **6MeNiNi** and reflects stabilisation of the mixed-valence state. The improvement in the donor abilities is caused by the intramolecular strain imposed by interactions between the methyl substituent and the macrocyclic ring.

The interaction between two metallic ions in the bismacrocyclic complexes that was found in the electrochemical studies in the **6MeCuCu** compound was also confirmed by ESR spectroscopy. This interaction is transmitted directly through space. It is also observed when the bridging chains become shorter for the **3MeCuCu** and **3CuCu** complexes.

According to solution $^1$H NMR titration results, the methylated receptors bind the π-donor guests more weakly then the nonmethylated ones. This is in good agreement with the directions of redox-potential changes. On the other hand, larger donors (naphthalene derivatives) have higher affinity towards both the **7NiNi** and **7MeNiNi** bismacrocycles. These observations confirm the π-donor···π-acceptor nature of the host–guest interactions and the usefulness of methylation in fine-tuning the properties of the cyclidene receptors. The introduction of small changes in the molecular structure of the compounds by such means as methylation or elongation of spacers leads to a significant modulation of the electrochemical and supramolecular properties.

## Acknowledgements

This work was financially supported by the State Committee for Scientific Research (Project no. 4T09A04823). The X-ray measurements were undertaken in the Crystallographic Unit of the Physical Chemistry Laboratory at the Chemistry Department of the University of Warsaw. The authors thank Prof. S. Szymański (Institute of Organic Chemistry, Polish Academy of Science, Warsaw, Poland) for helpful discussion about the NMR results. S.D. and K.W. are very grateful to the Polish State Committee for Scientific Research for its support through project no. 3T09A01828.

[1] D. W. Steuerman, H.-R. Tseng, A. J. Peters, A. H. Flood, J. O. Jeppesen, K. A. Nielsen, J. F. Stoddart, J. R. Heath, *Angew. Chem.* **2004**, *116*, 6648–6653; *Angew. Chem. Int. Ed.* **2004**, *43*, 6486–6491.
[2] S. S. Jang, Y. H. Jang, Y.-H. Kim, W. A. Goddard III, A. H. Flood, B. W. Laursen, H.-R. Tseng, J. F. Stoddart, J. O. Jeppesen, J. W. Choi, D. W. Steuerman, E. Delonno, J. R. Heath, *J. Am. Chem. Soc.* **2005**, *127*, 1563–1575.
[3] Y. Liu, A. H. Flood, J. F. Stoddart, *J. Am. Chem. Soc.* **2004**, *126*, 9150–9151.
[4] A. H. Flood, J. F. Stoddart, D. W. Steuerman, J. R. Heath, *Science* **2004**, *306*, 2055–2056.
[5] B. Korybut-Daszkiewicz, A. Więckowska, R. Bilewicz, S. Domagała, K. Woźniak, *J. Am. Chem. Soc.* **2001**, *123*, 9356–9366.
[6] A. Więckowska, R. Bilewicz, S. Domagała, K. Woźniak, B. Korybut-Daszkiewicz, A. Tomkiewicz, J. Mroziński, *Inorg. Chem.* **2003**, *42*, 5513–5522.
[7] B. Korybut-Daszkiewicz, A. Więckowska, R. Bilewicz, S. Domagała, K. Wozìniak, *Angew. Chem.* **2004**, *116*, 1700–1704; *Angew. Chem. Int. Ed.* **2004**, *43*, 1668–1672.
[8] D. H. Busch, N. W. Alcock, *Chem. Rev.* **1994**, *94*, 585–623.
[9] F. Devínsky, I. Lacko, L. Krasnec, *Synthesis* **1980**, *4*, 303–305.
[10] R. Ballardini, V. Balzani, J. Becher, A. Di Fabio, M. T. Gandolfi, G. Mattersteig, M. B. Nielsen, F. M. Raymo, S. J. Rowan, J. F. Stoddart, A. J. P. White, D. J. Williams, *J. Org. Chem.* **2000**, *65*, 4120–4126.
[11] Oxford Diffraction, CrysAlis CCD and CrysAlis RED, Oxford Diffraction Poland, Wrocław, Poland, **2001**.
[12] G. M. Sheldrick, *Acta Crystallogr. Sect. A* **1990**, *46*, 467–473.
[13] G. M. Sheldrick, SHELXL93, Program for the Refinement of Crystal Structures, University of Göttingen, Germany, **1993**.
[14] *International Tables for Crystallography, Vol. C* (Ed.: A. J. C. Wilson), Kluwer, Dordrecht, **1992**.
[15] T. J. Meade, C. M. Fendrick, P. A. Padolik, C. E. Cottrell, D. H. Busch, *Inorg. Chem.* **1987**, *26*, 4252–4257.
[16] R. R. Gagne, C. A. Koval, T. J. Smith, M. C. Cimolino, *J. Am. Chem. Soc.* **1979**, *101*, 4571–4580; R. R. Gagne, C. L. Spiro, T. J. Smith, C. A. Hamann, W. R. Thies, A. K. Shiemke, *J. Am. Chem. Soc.* **1981**, *103*, 4073–4081.
[17] J. J. Girerd, E. Anxolabbehere-Mallart in *Spectroscopic Methods in Bioinorganic Chemistry* (Eds.: E. I. Solomon, K. Hodgson), American Chemical Society, Washington, DC, **1997**, pp. 262–271.
[18] a) J. A. Weil, J. R. Bolton, J. E. Wertz, *Electron Paramagnetic Resonance*, Wiley, New York, **1992**; b) J. Szydłowska, A. Jurkiewicz, A. Krówczyński, *Liq. Cryst.* **2004**, *31*, 1655–1662; c) A. Krowczyński, D. Pociecha, J. Szydłowska, J. Przedmojski, E. Górecka, *Chem. Commun.* **1996**, 2731–2732.
[19] K. A. Connors, *Binding Constants: The Measurement of the Complex Stability*, Wiley, New York, **1987**.

Received: July 5, 2005
Revised: October 20, 2005
Published online: January 25, 2006

  